

Highly-collimated, high-charge and broadband MeV electron beams produced by magnetizing solids irradiated by high-intensity lasers

Cite as: Matter Radiat. Extremes 4, 044401 (2019); doi: 10.1063/1.5082330

Submitted: 20 November 2018 • Accepted: 12 March 2019 •

Published Online: 8 May 2019










View Online



Export Citation



CrossMark

S. Bolaños,¹  J. Béard,²  G. Revet,^{1,3}  S. N. Chen,^{1,3,4}  S. Pikuz,^{5,6}  E. Filippov,^{5,6}  M. Safronova,³
M. Cercez,⁷ O. Willi,⁷ M. Starodubtsev,³ and J. Fuchs^{1,3,4,a)} 

AFFILIATIONS

¹ LULI—CNRS, Ecole Polytechnique, CEA: Université Paris-Saclay; UPMC Univ Paris 06: Sorbonne Universités, F-91128 Palaiseau Cedex, France

² LNCMI, UPR 3228, CNRS-UGA-UPS-INSA, 31400 Toulouse, France

³ Institute of Applied Physics, 46 Ulyanov Street, 603950 Nizhny Novgorod, Russian Federation

⁴ ELI-NP, “Horia Hulubei” National Institute for Physics and Nuclear Engineering, 30 Reactorului Street, RO-077125 Bucharest-Magurele, Romania

⁵ Joint Institute for High Temperatures, RAS, 125412 Moscow, Russian Federation

⁶ National Research Nuclear University MEPhI, 115409 Moscow, Russian Federation

⁷ Institute for Laser and Plasma Physics, University of Düsseldorf, Düsseldorf, Germany

a) julien.fuchs@polytechnique.fr

ABSTRACT

Laser irradiation of solid targets can drive short and high-charge relativistic electron bunches over micron-scale acceleration gradients. However, for a long time, this technique was not considered a viable means of electron acceleration due to the large intrinsic divergence ($\sim 50^\circ$ half-angle) of the electrons. Recently, a reduction in this divergence to 10° – 20° half-angle has been obtained, using plasma-based magnetic fields or very high contrast laser pulses to extract the electrons into the vacuum. Here we show that we can further improve the electron beam collimation, down to $\sim 1.5^\circ$ half-angle, of a high-charge (6 nC) beam, and in a highly reproducible manner, while using standard stand-alone 100 TW-class laser pulses. This is obtained by embedding the laser-target interaction in an external, large-scale (cm), homogeneous, extremely stable, and high-strength (20 T) magnetic field that is independent of the laser. With upcoming multi-PW, high repetition-rate lasers, this technique opens the door to achieving even higher charges (>100 nC).

© 2019 Author(s). All article content, except where otherwise noted, is licensed under a Creative Commons Attribution (CC BY) license (<http://creativecommons.org/licenses/by/4.0/>). <https://doi.org/10.1063/1.5082330>

INTRODUCTION

The acceleration of electrons from plasmas has been actively pursued since the seminal work of Tajima and Dawson,¹ due to its very desirable characteristics and promising prospects. Indeed, since acceleration gradients in the plasma are orders of magnitude higher than those in conventional accelerator structures powered by microwaves,² the overall process is intrinsically extremely compact. It can also offer other advantages, depending on the particular scheme that is exploited, i.e., a high repetition rate, good collimation, high energy, and high charge.

Very varied schemes have been pursued to accelerate electrons from plasmas. One such scheme exploits low-density plasmas and intense lasers as the driver, the latter exciting a plasma wave that accelerates the electrons.³ The plasma wave can be excited in the wake of beat frequencies lasers,⁴ or in the wake of an intense, short laser pulse.⁵ Another low-density plasma scheme generates a cavity void of electrons, in the so-called bubble regime, i.e., in the wake of an ultra-intense, ultra-short laser pulse.² These techniques, especially the latter, have been shown to be very effective, producing narrow-spectrum, multi-giga electronvolt,⁶ collimated, and ultra-short⁷

electron beams, and there is now the prospect of stacking acceleration stages to further increase beam energy.⁸ Alternatively, the excitation of a plasma wave, again in a low-density plasma, induced by an externally injected particle beam has also been investigated in order to boost electron energy.^{9–11} Electron beams produced in low-density plasmas are well collimated, but the typical charge that can be extracted is, however, limited to around 10–100 pC. Note that magnetizing this setup has been shown to lead to enhanced collimation and charge.¹²

In order to increase the charge of the electron beam to or above the nanocoulomb level, i.e., to charges comparable to, or even higher than, those achieved by conventional accelerators, a second scheme of electron acceleration can be used. This scheme relies on the extraction and acceleration of electrons from high-density plasmas. Exciting a plasma wave in a solid-density target, in the wake of a short and intense X-ray pulse, has been proposed,¹³ but this is still beyond existing experimental capabilities. Rather, current practical methods exploit the acceleration, by an optical laser pulse, of electrons close to the critical density, i.e., at the point where pulse propagation is stopped. This can be done in two main ways: (i) by the direct acceleration of electrons, or (ii) by the excitation of a plasma wave in a high-density plasma that will in turn accelerate the electrons.^{14,15}

The direct acceleration of electrons to relativistic energies, using standard ultra-intense lasers, can be done inwardly through the target, using various mechanisms like $j \times B$,¹⁶ or the Brunel effect,^{17,18} or outwardly, in the vacuum.^{19,20} In the latter case, electrons are extracted from the target and are again accelerated in vacuum by reflected laser beam over a Rayleigh length (in the laser focal volume). In all cases, electrons are accelerated by irradiating an intense laser pulse on a solid target. The electrons are accelerated along the gradient in front of the target, in variable inward directions depending on the plasma gradient at the target surface,²¹ or along the laser specular direction for vacuum acceleration. For acceleration mediated by a plasma wave, a grazing incidence is usually used.

Note that a proportion of these relativistic electrons will be able to escape the target,²² but most of them will be retained, inducing electrostatic acceleration of protons and ions to mega electronvolt energies.²³ Thus, the escaping relativistic electrons will be followed by a neutralized plasma beam in which the ions are co-moving with the electrons. These electrons are slowed down to kilo electronvolt after having quickly (over a few hundreds of microns²⁴) transferred their energy to the ions. We will not focus here on the low-energy electrons within this plasma beam but rather on the forefront relativistic electrons.

In the case of direct acceleration of the electrons, the typical results obtained so far are as follows: For inward acceleration, the electron spectrum is typically Boltzmann-like, with a temperature (or mean energy) of 900 keV and a maximum energy around 3 MeV for a typical laser intensity of $I_L = 10^{19}$ W/cm².^{25,26} Note that in an idealized 1D model, the maximum energy of the accelerated electrons would be given as $a_0^2/2$, with a_0 being the normalized vector potential, $a_0 = (I_L \lambda_L^2 / 1.37 \times 10^{18} \text{ W } \mu\text{m}^2 \text{ cm}^{-2})^{1/2}$, and λ_L the laser wavelength, but that the stochastic nature of the laser-plasma interactions in 3D can lead the maximum electron energy to be several times that value in practice.^{27,28} The inwardly accelerated electrons present a strong divergence, where the half-angle of the spreading cone is around 50°

(~900 mrad).^{29,30} In order to collimate the inwardly accelerated electrons, a wave guide³¹ or surface magnetic field, driven by an auxiliary long-pulse laser,³⁰ has been proposed. The first method is, however, only effective while the electrons stay within the target, while the second can, at best, reduce the divergence to a half-angle of ~10° (175 mrad),³⁰ due to the very limited influence of the laser-driven magnetic fields beyond the target surface.³² Outwardly accelerated electrons (i.e., in vacuum) exhibit a similar divergence¹⁹ (half-angle of 17°, or 300 mrad, for a similar laser intensity $I_L = 2 \times 10^{19}$ W/cm²). In this case, the electron energy is also slightly larger than that of the inwardly accelerated electrons, i.e., a few tens of MeV. Note that the outward vacuum acceleration scheme relies on the use of very high contrast laser pulses, which generally requires resorting to plasma mirrors temporal cleaning. Regardless, in both cases, inward or outward, charges greater than nanocoulomb are achieved.

In order to simultaneously simplify both schemes discussed above and improve their performances in terms of collimation, we propose and demonstrate here a scheme where we still exploit magnetic collimation but use an externally applied field, the advantages of which are its long length of application and its uniformity. Contrary to vacuum acceleration, this scheme does not require high-contrast pulses and the associated need for a dedicated plasma mirror system; imperfect laser temporal contrast is even desired to increase laser absorption efficiency.³³ This compact setup of Magnetized Laser Acceleration (MALA) is simply achieved by coupling a laser-solid interaction with a strong (20 T³⁴) external axial magnetic field. At an intensity of $I_L \sim 10^{19}$ W/cm² and a laser energy ~10 J, we show that this scheme can collimate efficiently down to a very low divergence (to a half-angle of ~25 mrad, or 1.5°) over long-distance (cm) MeV electrons. These electrons have been accelerated inward the solid target by the laser, are expelled on the target rear and are focused by the large-scale magnetic field. We measure in our conditions that a charge of ~6 nC of electrons can be this way collimated, without any loss of energy during collimation.

EXPERIMENTAL SETUP

The experiment was conducted at the ELFIE facility of the LULI laboratory (Palaiseau, France). The facility is equipped with a 100 TW laser³⁵ which provides laser pulses, based on Chirped-Pulse-Amplification (CPA) technology,³⁶ at a central wavelength, $\lambda = 1.058$ μm , with an energy, per pulse, on target $E = 9$ J and a FWHM duration $\tau_{laser} = 400$ fs after compression. This laser, using flash lamps as amplifiers, has a low repetition rate of one shot per 20 min, but more modern lasers of similar power can achieve a 10 Hz repetition rate.³⁷ Since the experiment we describe here was performed at the fundamental wavelength, the interaction with the solid did not take place in the high-contrast regime, i.e., a preplasma with a low-density tail $\exp(-x/L)$, with $L \sim 50$ μm ,³⁸ is present at the target front at the time of the short-pulse arrival. This preplasma is induced by the ~1 ns duration, 10^{12} W/cm² intensity amplified spontaneous emission (ASE) preceding the main laser pulse.³⁹

As illustrated in Fig. 1, the laser beam is focused at normal incidence on the solid targets with an $f/3$ off-axis parabola, resulting in a spot size on the target of 11 μm FWHM and a peak intensity $I \sim 10^{19}$ W/cm² corresponding to an associated normalized vector potential $a_0 \sim 2.8$. The solid targets are 23 μm -thickness foils composed of aluminized Mylar (i.e., a 0.2 μm Al layer is deposited on a

22.8 μm Mylar substrate, with the Al layer being on the laser-irradiated side). The target is placed at the center of a Helmholtz-type coil in order to embed the laser-target interaction in a large-scale, long-duration magnetic field (see below).

The coil was developed at the LNCMI laboratory (Toulouse, France). It is placed at the center of the evacuated target chamber, as shown in Fig. 1, through a re-entrant tube. A tube, welded within the coil, allows the laser beam to propagate unimpeded to the center of the coil and to reach the target which sits in vacuum, while the rest of the coil is exposed to the air for cooling after the shot (full details on the operation of the coil are given in Ref. 40). Note that here we used passive air cooling as we did not work at a high repetition rate, but that active cooling, e.g., with a flow of liquid nitrogen, would have provided the possibility of using this system at a high repetition rate. The normal of the target was positioned along the coil axis (see Fig. 1). The coil was easily able to generate a 20 T magnetic field of more than 4 cm along the field axis, with a 1 cm diameter, i.e., radially (see the field distribution detailed in Fig. 2 of Ref. 40). The rise time of the coil was 190 μs , meaning that the magnetic field was constant over the electron beam

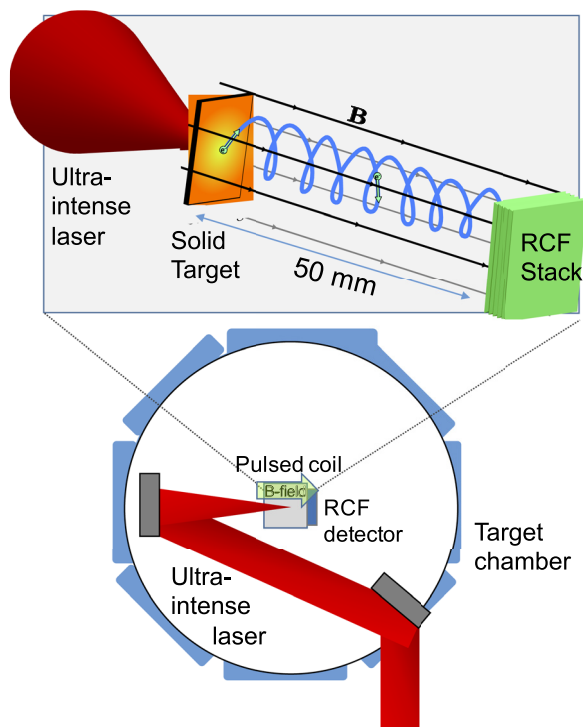


FIG. 1. Schematic experimental setup illustrating the geometry of laser irradiation on the target. The foil is positioned at the center of the coil assembly where the laser is focused and where the collimating pulsed magnetic field is driven by the pulsed coil. To diagnose the electrons, a stack of RCF is placed at the output of the coil, on the opposite side of the entrance where the laser beam enters the coil. Inset: the principle of collimation, by the magnetic field, of the electrons accelerated from the solid target by the high-intensity laser beam, up to the detector (RCF stack, see text for details). The electrons are affected by the external magnetic field (the black arrowed lines represent magnetic field lines) so they gyrate around the magnetic field lines, moving with helical trajectories, one of which is represented by the blue line.

generation and propagation timescales ($< \text{ns}$). Note that variation of the current delivered to the coil, and hence variation of the magnetic field, was very small, $< 0.5\%$, which resulted in a very high stability of the collimation imposed on the electrons, as will be shown below.

A stack of Gafchromic™ films (RCF),⁴¹ positioned right at the edge of the coil assembly (see Fig. 1), i.e., 5 cm away from the target, was used as the main diagnostic to characterize the electron beam, since it could provide information about the spatial distribution of the beam as well as its energy distribution. In order to filter out the laser light and plasma emission, an aluminum filter was placed in front of the RCF stack. Filter thickness was varied from 12.5 μm to 2.5 mm between shots in order to further discriminate between electron and proton signals observed in the RCF. Protons require an energy of at least around 22 MeV to go through 2.5 mm of aluminum, but we recorded, under these experimental conditions, a maximum proton energy of only 12 MeV.⁴² Note that the proton beam following the relativistic electrons is also impacted by the magnetic field, but less so due to the proton's higher mass. Magnetic solenoids can thus be used to collimate laser-accelerated protons, but with a limited capture efficiency of the initially divergent beam.⁴³ This is in contrast to a solenoid's effect on an electron beam, even though the electrons are initially more divergent than the protons,⁴⁴ electrons can be fully captured by the magnetic focusing structure due to the low electron mass, as will be detailed below.

Thus, using the thick filter allowed us to block protons and analyze the electron spectrum in isolation. This was at the expense, however, of increased Coulomb scattering of the electrons by the thick filter. Hence, the thin filter stack, which induced less scattering, was also used in order to better record the intrinsic electron beam profile. Using the thin filter, we could readily discriminate between electrons and protons, as the protons, having a sharp energy deposition profile, penetrated only the first few layers of the RCF stack, while the electrons penetrated much more deeply.

RESULTS

Figure 2(a) shows the recorded electron spectrum, retrieved from the RCF, and the angular beam pattern [see the inset of Figs. 2(a) and 2(b)] observed on the RCF, at 5 cm away from the target, within the 20 T magnetic field. We emphasize that no signal could be observed on the same films in the absence of the magnetic field, the electrons having such a wide divergence²⁹ that their dose at the film location could not be distinguished from the background, i.e., the simultaneous X-rays generated as the result of laser irradiation of the target.

The spectrum shown in Fig. 2(a) is inferred from the RCF stack as follows: First, using the calibration of the RCFs reported by Chen *et al.*,⁴¹ the dose deposited by the electrons in each film of the stack can be retrieved by integrating over the whole signal imprinted on each RCF. Then, the energy spectrum of the electrons is inferred by starting from a given (Boltzmann-like) spectrum, simulating the electron deposition in the RCFs, and then comparing the simulated deposited dose to the experimentally measured one. The simulated energy deposition in the RCFs is computed using the electron stopping power given by the ESTAR database.⁴⁵ The initial spectrum is progressively modified until a best fit is found with the measured dose across the RCFs. The spectra resulting from this procedure, for two different shots [one with the thin Al filter (in black), the other with the

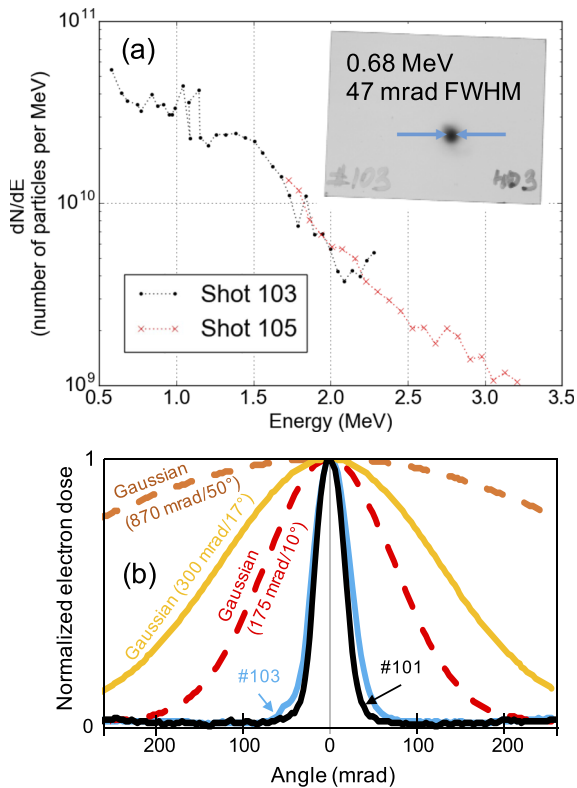


FIG. 2. Experimental evidence for highly charged, broadband and collimated mega electronvolt electron acceleration. Panel (a) shows the spectrum inferred from the RCF film stacks for two different laser shots. For shot 103 (black dotted line with point markers), a 12.5 μm -thick aluminum filter has been placed in front of the RCF stack to protect it; however, for shot 105 (red dotted line with cross markers), a 2.5 mm-thick aluminum filter has been placed there to protect the stack. Because of varied Al filter thickness, the two RCF stacks do not probe the same range of electron energies. The two spectra present a Boltzmann distribution with a hot electron temperature, $T_{\text{hot}} = 0.68$ MeV. Integrating over the range of energies shown in panel (a), we obtain for the electron beam a total charge of $Q = 6.1$ nC. Inset: raw scanned RCF film from shot 103 corresponding to a mean energy of the incident electrons, which imprinted the film, that is equal to the average energy of the electrons in the distribution (i.e., 0.68 MeV). Panel (b): angular distribution of the electron dose (normalized) as measured from the RCF, again corresponding to electrons having a mean energy of 0.68 MeV, and for two different shots (#101 and #103). The plots represent the dose vs angle as measured from a lineout of the RCF at a given angle. We have checked that the beam profile was very symmetric [as can be seen in the inset of panel (a)], meaning that the lineout did not depend significantly on the choice of angle. Overlaid are Gaussian angular distributions having a FWHM of $10^\circ/175$ mrad, and of $50^\circ/870$ mrad. These represent the results reported in Ref. 30 for, respectively, the cases of magnetic collimation of electrons and uncollimated electrons. Also shown is a Gaussian angular distribution having a FWHM of $17^\circ/300$ mrad, representing the results concerning vacuum laser acceleration of electrons, reported in Ref. 19.

thick Al filter (in red)], are shown in Fig. 2(a). One can observe a good reproducibility of the retrieved electron spectrum between these two shots. Note also that, as shown in earlier studies,^{22,46,47} the energy spectrum of the electrons collected far from the target is representative of that derived from the electrons accelerated by the laser at the target interface. The spectra shown in Fig. 2(a) can be fitted by a Boltzmann

distribution $dN/dE = \exp(-E/T_{\text{hot}})$ with $T_{\text{hot}} = 0.68$ MeV, which thus represents the average energy of the electrons within the beam.

In our moderate intensity and moderate temporal contrast regime, several models and scalings exist for the hot electron temperature produced by laser-solid interactions. The empirical scaling of Beg,²⁵ supported by Haines' model,²⁶ gives T_{hot} (MeV) = $0.215 (I_{18} \lambda_{\mu\text{m}}^2)^{1/3}$, i.e., 0.46 MeV under our conditions. Alternatively, the ponderomotive scaling established by Wilks *et al.*¹⁶ gives T_{hot} (MeV) = $0.511 [(1 + a_0^2)^{1/2} - 1]$, i.e., 1 MeV in our case. Note that these formulas assume that the entire energy of the laser is transferred to the solid target, i.e., that the reflectance is zero. This assumption could explain the discrepancy between the temperature we retrieved from our spectra and that from the ponderomotive scaling, i.e., accounting for some reflected light (not measured here) would reduce the temperature predicted by the ponderomotive scaling.

Fitting the electron spectrum does not only yield an estimate of T_{hot} , but also, by integrating the spectrum over the energies, yields the total number of electrons contained within the beam, and hence, the total charge in the beam. By performing the integration, we find that the total charge of the electrons able to escape the target is $Q_{\text{tot}} = 6.1$ nC. This number is comparable to the charge measured from the best results obtained in other experiments aimed at analyzing and measuring electron beams that can be driven by a laser, i.e., from a few to tens of nC.⁴⁸ Note that here we did not account, in the charge integration, for electrons having an energy lower than 0.5 MeV.

The collimation imposed by the external magnetic field (20 T) on the expelled electron bunch is illustrated by the narrow angular profile of the electron beam, as recorded by the RCF in 2D (in the plane transverse to electron propagation, see Fig. 1) and as shown in Fig. 2(b). On the RCF of the inset of Fig. 2(a), which corresponds to electrons having an energy equal to the average energy of the distribution (i.e., 0.68 MeV), the measured divergence (FWHM) is only ~ 47 mrad. We verified that, in this case, the observed divergence is not induced by multiple scatterings of the electrons within the 12.5 μm -thick Al filter. This was done using the Highland formula,⁴⁹ which is relevant for the electron energies considered here and the thickness of the Al filter: the divergence induced by multiple scatterings in the filter is negligible compared to the measured beam divergence.

Shown in Fig. 2(b) are also the comparative electron beam angular divergences reported in previous studies: $10^\circ/175$ mrad FWHM divergence (electrons collimated by laser-driven magnetic fields³⁰); $17^\circ/300$ mrad FWHM divergence (vacuum accelerated electrons¹⁹); and $50^\circ/850$ mrad FWHM divergence (uncollimated electrons³⁰). Note that these are all half-angle divergences, and we have deliberately interpreted them favorably (i.e., underestimating the beam divergence) as a FWHM. As shown in Fig. 2(b), our setup provides significantly better collimation for the electrons, and reproducibility of the results is also quite good.

To verify that the magnetic field, having quasi-parallel lines within the coil [as shown in Fig. 3(b)], allows collimation after the widely divergent electrons are ejected from the solid target, we simulated, using SIMION software,⁵⁰ the propagation of electrons within the external magnetic field generated by the Helmholtz coil. Using the measured spectra of the electrons, shown in Fig. 2(a), and an assumed angular distribution (detailed below), SIMION is able to calculate the trajectories of the electrons in a given magnetic field. The magnetic field used in the calculation corresponds to the experimental

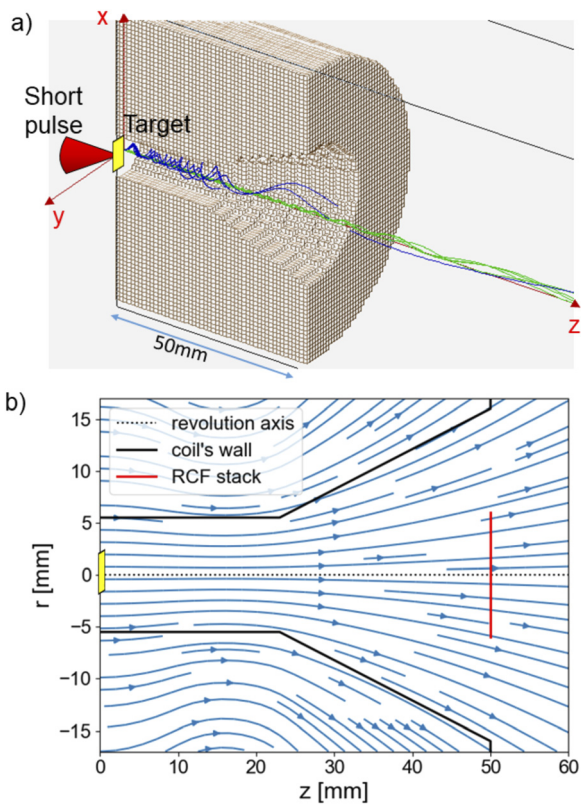


FIG. 3. SIMION calculations of the collimation process: Panel (a) shows the propagation of electrons in an electromagnetic field. The brown mesh represents the body of the coil used in our experiment to induce collimation of the laser-accelerated electrons. The helical lines in blue and green represent the trajectories of 10 MeV electrons launched from the source target, with different initial angles of direction, i.e., 15° to the propagation axis X (in green) and 45° to the propagation axis X (in blue). Panel (b) represents the magnetic field lines in the YZ plane. The slow spatial gradient of the magnetic field, having quasi-parallel lines, compared to the short Larmor radius of the electrons rotating within the B-field explains the good collimation ability of the setup. The black solid lines represent the coil's wall.

one, with respect to its spatial distribution, and strength, $B = 20$ T, as also measured during the experiment using a Rogowski coil. We assume that the magnetic field is constant over time since the time-scale of the magnetic field evolution is negligible compared to the time spent by the electrons before they reach the RCF. **Figure 3** presents two different views of the calculations performed using SIMION. In **Fig. 3(a)**, the brown mesh represents the walls of the coil. The green lines represent sample helical trajectories of electrons with a kinetic energy $K = 10$ MeV and an initial angle to the propagation axis (X in the simulation) $\theta = 15^\circ$. The blue lines represent the same, but for a different initial angle to the propagation axis, i.e., $\theta = 45^\circ$. We observe that the Larmor radius of the electrons [as illustrated in **Fig. 3(a)**] is much shorter than the spatial gradient of the magnetic field [see **Fig. 3(b)**]. This explains this setup's capability to impose a tight collimation on the electrons.

Simulations were performed for various electron kinetic energies to check the influence of the magnetic field on the overall spectrum of the electron beam. Because the simulation mesh is axisymmetric with

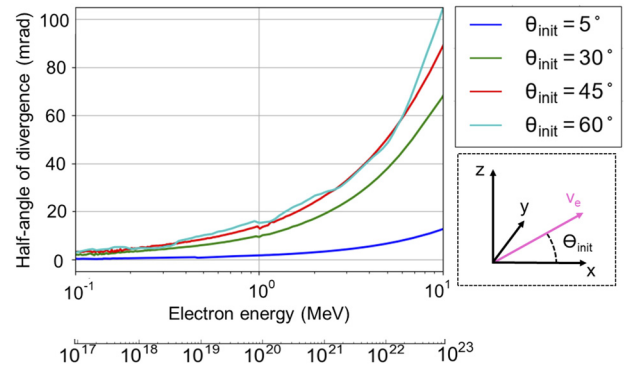


FIG. 4. SIMION simulations of the final divergence, θ , of the electron beam as a result of propagation in the magnetic field structure, for various initial divergences, θ_{init} , of the electrons leaving the target (as shown in the inset) and various electron energies (see text for details). The divergence is computed past the exit of the coil, i.e., once the electrons are freely drifting away.

respect to the propagation axis [i.e., the X axis, see **Fig. 3(a)**], we varied only the initial direction of the electrons, with respect to the propagation axis, which is the θ angle depicted in the coordinates cartoon of **Fig. 4**. As a reference, when $\theta = 0^\circ$, the initial velocity vector of the sampled electron, \vec{v}_e , is collinear with the propagation axis. Moreover, and as shown in **Fig. 3**, only half of the magnetic field coil has been implemented in the SIMION simulation, since the electrons propagate along the positive part of the X axis only, and their origin is coincident with the center of the coil, where the laser-irradiated source foil is positioned.

As mentioned above, it has been shown that laser generation of electrons at the target front in an interaction regime relevant for our conditions is characterized by an injection into the target with a divergence (half-angle) of up to 50° .^{29,30} Therefore, in order to ensure we were not underestimating the divergence at the source, we varied, in SIMION, the initial angle, θ , of the electrons leaving the source target from 0° to 60° .

Figure 4 summarizes the results of the SIMION calculations. Shown as ordinates is the final electron divergence, after the electrons freely propagate away from the coil. This is plotted for electrons with various θ and kinetic energies ranging from 100 keV to 10 MeV (as represented by the abscissae). The electron energies in the abscissae can also be seen as the average energy of electrons within the distribution, which is given by the hot electron temperature, T_{hot} , function of the laser intensity. Thus, we also indicate in the abscissae the corresponding laser intensity using Beg's law as a correspondence between T_{hot} and the laser intensity. Obviously, for $\theta = 0^\circ$, where electrons are collinear with the magnetic field, the Lorentz force is zero, and the electrons propagate straight forward.

When compared with the measurement of **Fig. 2(b)**, we see that the SIMION simulation yields quite a low divergence compared with what we measured. This demonstrates that the magnetic field setup used here is indeed able to induce very strong collimation, even of an initially very divergent electron beam and even at very high laser intensities, i.e., at high average electron energies (T_{hot}). Note that the SIMION calculations show that for electron energies of over 20 MeV, some of the electrons crash on the coil, which has an opening angle of $\theta = 27^\circ$. Thus, in our case, since we measured the maximum electron energy to be 3.2 MeV, all electrons ejected from

the target in the experiment were indeed collimated, and none of them were lost on their way toward the RCF stack. We therefore conclude that the electron beam spectrum is not altered during propagation through the coil.

Thus, we attribute the observed divergence of the electron beam to space-charge effects. Note indeed that the relativistic electrons are ahead of the slower plasma beam mentioned above (typically, a 5 MeV proton has a velocity $\sim 0.1c$), and are hence un-neutralized. Analytically estimating the electrostatic repulsive force that would make the electron beam swell yields a beam expansion of the same order of magnitude (~ 100 mrad) as that from observation. We expect that the divergence will increase with electron energy, as the collimating effect induced by the B field reduces.

CONCLUSION AND OUTLOOK

The comparative characteristics of electron beams produced by existing acceleration techniques, alongside those of the beam produced by the MALA mechanism highlighted in this paper are summarized in Table I. The various mechanisms listed can generate an electron beam with very broad and diverse specifications, from monochromatic (e.g., Wakefield and LINAC) to Maxwellian-like (e.g., MALA) spectra, and from very high energy electrons (e.g., Wakefield) to a high-charge beam (e.g., VLA and MALA). The solid target-laser interaction-based mechanisms, VLA and MALA, present similar characteristics, the main difference being the beam divergence. The VLA drives a more divergent electron beam, 300 mrad, compared with the MALA setup presented here, where we achieve a divergence of around 50 mrad.

With the upcoming multi-petawatt-class laser facilities, such as Apollon⁵³ or the European Extreme Light Infrastructure (ELI) facilities,⁵⁴ the setup proposed in this paper could provide an interesting and easily implementable secondary source of electrons. With these facilities, working at a wavelength of $0.8 \mu\text{m}$, it is expected at the highest power of 10 PW that the intensity at focus will reach up to $I_L \sim 10^{22} \text{ W/cm}^2$ (with a pulse duration ~ 20 fs), with an associated normalized vector potential $a_0 \sim 70$. According to Beg's scaling, the hot electron temperature would then reach up to $T_{\text{hot}} \sim 4$ MeV. In order to vary the latter, the laser pulse could also be stretched in time, e.g., to 400 fs, in which case the intensity would be $\sim 5 \times 10^{20} \text{ W/cm}^2$ ($a_0 \sim 15$) and the hot electron temperature $T_{\text{hot}} \sim 1.5$ MeV, according to Beg's scaling. We note that in order to make our scheme compatible with the high repetition rates

of these facilities, our scheme could exploit liquid or cryogenic gas based targets.^{42,55}

According to the analytical and experimental studies reported by Dubois *et al.*⁴⁸ and Poyé *et al.*,⁵⁶ it is possible to estimate the charge of the electron beam depending on the laser pulse duration and the hot electron temperature (or the laser intensity). By definition, the total charge can be calculated via the integration over time of the current driven by the ejected electrons. The current is constant during the laser pulse duration, as laser intensity is assumed to be constant. At the end of the laser pulse, the hot electron temperature decreases due to electron-electron collisions. During this cooling time, electrons are still ejected but their number decreases significantly, reducing the current. Hence, the ejected-electron current depends predominantly on the hot electron temperature, and for a constant laser pulse duration, the total charge increases with laser energy. Conversely, for a constant laser energy, the ejected electron charge is not observed to vary with varying laser pulse duration. At facilities such as Apollon, the pulse energy will be in the order of 200 J. At such an energy, simulations reported by Link *et al.*²² showed that the escaping electrons carry away $\sim 4\%$ of the laser energy. Assuming that the laser absorption at the above-mentioned intensities was quasi total, as shown by Ping *et al.*,⁵⁷ this would have led to a charge for the escaping electrons of ~ 120 nC for 200 J of laser energy. We must note that, as discussed above, not all escaping electrons will be collimated by the magnetic field, since those with energies above 20 MeV will crash into the coil's wall. Such a limitation will reduce the collimated-beam charge, albeit only slightly: for an electron beam with $T_{\text{hot}} \sim 4$ MeV, the total charge will only be reduced by $\sim 0.7\%$. We note that such a high charge would certainly impact the divergence of the beam. A quantitative estimate of this effect can be obtained using existing numerical codes,^{58,59} but since the space charge forces are linear, the emittance growth induced by the forces is totally reversible and, as a consequence, can be compensated for, as shown by test facilities using very high-charge beams, e.g., up to 100 nC.⁶⁰

Regarding possible applications, we envisage that the production of very high-charge beams using the MALA scheme could be interesting in three main respects: (i) as a compact, high-charge electron injector for conventional accelerators,⁶¹ or (ii) for the production of bright gamma-rays, using a converter, in order to probe dense materials.⁶² We note here that gamma-ray production using electron beams produced by solids, possessing similar temperatures as discussed above, albeit at a lower dose, has already been tested⁶³ and shown to be relevant for material probing.⁶⁴ Increasing the charge of

TABLE I. Overview of comparative parameters produced by various electron acceleration schemes and the expected parameters using upcoming multi-PW lasers (in italics). Here, we note that the maximum energy of the electrons in the MALA scheme using 10 PW lasers is effectively limited to 20 MeV, since higher energy electrons will crash onto the coil's wall. The notation "RF" refers to the radio-frequency gun used as the injector in a LINAC.

	Laser wakefield ²	Vacuum laser acceleration (VLA) from solids using high-contrast laser pulses ¹⁹	Magnetized laser acceleration (MALA) from solids (this work)	<i>MALA—Expected using 10 PW lasers</i>	LINAC ^{51,52}
Charge	100 pC	12 nC	6 nC	<i>~ 120 nC</i>	1 nC
Divergence	2–10 mrad	300 mrad	50 mrad	<i>...</i>	Emittance rms = $1.2 \mu\text{m}$
E_{max}	Few GeVs	$E_{\text{peak}} = 10$ MeV	4 MeV	<i>20 MeV (effective)</i>	5 MeV (RF) 14 GeV
Average energy			0.68 MeV	<i>1.5–4 MeV</i>	
Spectrum type	Narrow band	Broadband	Power law	<i>Power law</i>	Narrowband

the electron beam would offer the obvious advantage of increasing the signal to noise ratio, compared with these early tests, and allowing single-shot imaging. A third possible application could be (iii) the use of low-energy electrons to perform electron diffraction with atomic scale and picosecond scale resolution.⁶⁵ For this third potential application, similarly as for the second one, increasing the charge compared with other schemes (e.g., conventional accelerators or laser wakefield), would increase the sensitivity of the method.

Finally, we also note that using very thin targets, instead of the thick targets used here, to generate electrons would permit the exploitation of a regime where the laser beam would be partially transmitted through the foil⁶⁶ while accelerating the electrons. In this case, by further using Hermite–Gaussian modes for the laser beam, calculations⁶⁷ suggest that electrons produced in such a partial-transparency regime could benefit from an energy boost when applying a strong axial magnetic field as used here. Thus, applying a magnetic field would not only collimate the electrons but also improve their energy.

ACKNOWLEDGMENTS

We thank the LULI technical teams for their expert support and fruitful discussions with L. Gremillet and X. Davoine (CEA). This work was partly done within the LABEX Plas@Par project. It was supported by Grant Nos. 11-IDEX-0004-02 and ANR-17-CE30-0026-Pinnacle from Agence Nationale de la Recherche. This project has received funding from the European Union's Horizon 2020 research and innovation program under Grant Agreement No. 654148 Laserlab-Europe and from the European Research Council (ERC) under the European Union's Horizon 2020 research and innovation program (Grant Agreement No. 787539). This work was supported by the Ministry of Education and Science of the Russian Federation under Contract No. 14.Z50.31.0007. The work of JIHT RAS team was done under financial support of the Russian Science Foundation (Grant No. 17-72-20272). The research leading to these results is supported by Extreme Light Infrastructure Nuclear Physics (ELI-NP) Phase I, a project co-financed by the Romanian Government and European Union through the European Regional Development Fund.

The data that support the findings of this study are provisionally available from the corresponding author upon request.

REFERENCES

- ¹T. Tajima and J. M. Dawson, "Laser electron accelerator," *Phys. Rev. Lett.* **43**, 267–270 (1979).
- ²V. Malka *et al.*, "Principles and applications of compact laser–plasma accelerators," *Nat. Phys.* **4**, 447–453 (2008).
- ³E. Esarey, C. B. Schroeder, and W. P. Leemans, "Physics of laser-driven plasma-based electron accelerators," *Rev. Mod. Phys.* **81**, 1229–1285 (2009).
- ⁴C. Joshi *et al.*, "Ultra-high gradient particle acceleration by intense laser-driven plasma density waves," *Nature* **311**, 525–529 (1984).
- ⁵F. Amiranoff *et al.*, "Observation of laser wakefield acceleration of electrons," *Phys. Rev. Lett.* **81**, 995–998 (1998).
- ⁶W. P. Leemans *et al.*, "Multi-GeV electron beams from capillary-discharge-guided subpetawatt laser pulses in the self-trapping regime," *Phys. Rev. Lett.* **113**, 245002 (2014).
- ⁷O. Lundh *et al.*, "Few femtosecond, few kiloampere electron bunch produced by a laser–plasma accelerator," *Nat. Phys.* **7**, 219–222 (2011).
- ⁸S. Steinke *et al.*, "Multistage coupling of independent laser-plasma accelerators," *Nature* **530**, 190–193 (2016).
- ⁹J. B. Rosenzweig *et al.*, "Experimental observation of plasma wake-field acceleration," *Phys. Rev. Lett.* **61**, 98–101 (1988).
- ¹⁰M. Litos *et al.*, "High-efficiency acceleration of an electron beam in a plasma wakefield accelerator," *Nature* **515**, 92–95 (2014).
- ¹¹E. Gschwendtner *et al.*, "AWAKE, the advanced proton driven plasma wakefield acceleration experiment at CERN," *Nucl. Instrum. Methods Phys. Res., Sect. A* **829**, 76–82 (2016).
- ¹²T. Hosokai *et al.*, "Effect of external static magnetic field on the emittance and total charge of electron beams generated by laser-wakefield acceleration," *Phys. Rev. Lett.* **97**, 075004 (2006).
- ¹³S. Hakimi *et al.*, "Wakefield in solid state plasma with the ionic lattice force," *Phys. Plasmas* **25**, 023112 (2018).
- ¹⁴Y. Tian *et al.*, "Electron emission at locked phases from the laser-driven surface plasma wave," *Phys. Rev. Lett.* **109**, 115002 (2012).
- ¹⁵L. Fedeli *et al.*, "Electron acceleration by relativistic surface plasmons in laser-grating interaction," *Phys. Rev. Lett.* **116**, 015001 (2016).
- ¹⁶S. C. Wilks, W. L. Kruer, M. Tabak, and A. B. Langdon, "Absorption of ultra-intense laser pulses," *Phys. Rev. Lett.* **69**, 1383–1386 (1992).
- ¹⁷F. Brunel, "Not-so-resonant, resonant absorption," *Phys. Rev. Lett.* **59**, 52–55 (1987).
- ¹⁸J. P. Geindre, R. S. Marjoribanks, and P. Audebert, "Electron vacuum acceleration in a regime beyond Brunel absorption," *Phys. Rev. Lett.* **104**, 135001 (2010).
- ¹⁹M. Thévenet *et al.*, "Vacuum laser acceleration of relativistic electrons using plasma mirror injectors," *Nat. Phys.* **12**, 355–360 (2016).
- ²⁰Y. Ma *et al.*, "Ultra-high-charge electron beams from laser-irradiated solid surface," *Proc. Natl. Acad. Sci. U. S. A.* **115**, 6980–6985 (2018).
- ²¹M. I. K. Santala *et al.*, "Effect of the plasma density scale-length on the direction of fast electrons in relativistic laser–solid interactions," *Phys. Rev. Lett.* **84**, 1459–1462 (2000).
- ²²A. Link, R. R. Freeman, D. W. Schumacher, and L. D. Van Woerkom, "Effects of target charging and ion emission on the energy spectrum of emitted electrons," *Phys. Plasmas* **18**, 053107 (2011).
- ²³P. Mora, "Plasma expansion into a vacuum," *Phys. Rev. Lett.* **90**, 185002 (2003).
- ²⁴S. N. Chen *et al.*, "Passive tailoring of laser-accelerated ion beam cut-off energy by using double foil assembly," *Phys. Plasmas* **21**, 023119 (2014).
- ²⁵F. N. Beg *et al.*, "A study of picosecond laser–solid interactions up to 10^{19} W cm⁻²," *Phys. Plasmas* **4**, 447–457 (1997).
- ²⁶M. G. Haines, M. S. Wei, F. N. Beg, and R. B. Stephens, "Hot-electron temperature and laser-light absorption in fast ignition," *Phys. Rev. Lett.* **102**, 045008 (2009).
- ²⁷A. V. Arefiev *et al.*, "Beyond the ponderomotive limit: Direct laser acceleration of relativistic electrons in sub-critical plasmas," *Phys. Plasmas* **23**, 056704 (2016).
- ²⁸B. S. Paradkar *et al.*, "Numerical modeling of fast electron generation in the presence of preformed plasma in laser–matter interaction at relativistic intensities," *Phys. Rev. E* **83**, 046401 (2011).
- ²⁹J. C. Adam, A. Héron, and G. Laval, "Dispersion and transport of energetic particles due to the interaction of intense laser pulses with overdense plasmas," *Phys. Rev. Lett.* **97**, 205006 (2006).
- ³⁰H. B. Zhuo *et al.*, "Collimation of energetic electrons from a laser–target interaction by a magnetized target back plasma preformed by a long-pulse laser," *Phys. Rev. Lett.* **112**, 215003 (2014).
- ³¹B. Ramakrishna *et al.*, "Laser-driven fast electron collimation in targets with resistivity boundary," *Phys. Rev. Lett.* **105**, 135001 (2010).
- ³²L. Lancia *et al.*, "Topology of megagauss magnetic fields and of heat-carrying electrons produced in a high-power laser–solid interaction," *Phys. Rev. Lett.* **113**, 235001 (2014).
- ³³A. S. Pirozhkov *et al.*, "Diagnostic of laser contrast using target reflectivity," *Appl. Phys. Lett.* **94**, 241102 (2009).
- ³⁴B. Albertazzi *et al.*, "Production of large volume, strongly magnetized laser-produced plasmas by use of pulsed external magnetic fields," *Rev. Sci. Instrum.* **84**, 043505 (2013).
- ³⁵J. P. Zou *et al.*, "Recent progress on LULI high power laser facilities," *J. Phys.: Conf. Ser.* **112**, 032021 (2008).

- ³⁶D. Strickland and G. Mourou, "Compression of amplified chirped optical pulses," *Opt. Commun.* **56**, 219–221 (1985).
- ³⁷U. Schramm *et al.*, "First results with the novel petawatt laser acceleration facility in Dresden," *J. Phys.: Conf. Ser.* **874**, 012028 (2017).
- ³⁸S. Buffechoux, Augmentation de l'énergie des faisceaux de protons accélérés par laser ultra-intense et l'étude des caractéristiques des faisceaux accélérés par laser ultra-court, Paris-Sud University, France, 2011, <https://tel.archives-ouvertes.fr/tel-00600647>.
- ³⁹M. Gauthier *et al.*, "Investigation of longitudinal proton acceleration in exploded targets irradiated by intense short-pulse laser," *Phys. Plasmas* **21**, 013102 (2014).
- ⁴⁰D. P. Higginson *et al.*, "Detailed characterization of laser-produced astrophysically-relevant jets formed via a poloidal magnetic nozzle," *High Energy Density Phys.* **23**, 48–59 (2017).
- ⁴¹S. N. Chen *et al.*, "Absolute dosimetric characterization of Gafchromic EBT3 and HDv2 films using commercial flat-bed scanners and evaluation of the scanner response function variability," *Rev. Sci. Instrum.* **87**, 073301 (2016).
- ⁴²S. D. Kraft *et al.*, "First demonstration of multi-MeV proton acceleration from a cryogenic hydrogen ribbon target," *Plasma Phys. Controlled Fusion* **60**, 044010 (2018).
- ⁴³S. Busold *et al.*, "Focusing and transport of high-intensity multi-MeV proton bunches from a compact laser-driven source," *Phys. Rev. Spec. Top.-Accel. Beams* **16**, 101302 (2013).
- ⁴⁴P. R. Bolton *et al.*, "Instrumentation for diagnostics and control of laser-accelerated proton (ion) beams," *Phys. Med.* **30**, 255–270 (2014).
- ⁴⁵M. J. Berger, J. S. Coursey, M. A. Zucker, and J. Chang, Stopping-Power & Range Tables for Electrons, Protons, and Helium Ions, <https://www.nist.gov/pml/stopping-power-range-tables-electrons-protons-and-helium-ions>, 1998.
- ⁴⁶P. Antici *et al.*, "Measuring hot electron distributions in intense laser interaction with dense matter," *New J. Phys.* **14**, 063023 (2012).
- ⁴⁷P. Mora and T. Grismayer, "Rarefaction acceleration and kinetic effects in thin-foil expansion into a vacuum," *Phys. Rev. Lett.* **102**, 145001 (2009).
- ⁴⁸J.-L. Dubois *et al.*, "Target charging in short-pulse-laser-plasma experiments," *Phys. Rev. E* **89**, 013102 (2014).
- ⁴⁹V. L. Highland, "Some practical remarks on multiple scattering," *Nucl. Instrum. Methods* **129**, 497–499 (1975).
- ⁵⁰See <https://simion.com> for SIMION software.
- ⁵¹S. Schreiber, "The injector of the VUV-FEL at DESY," in *Proceedings of FEL (2005)*, Vol. 27, pp. 545–548, available at accelconf.web.cern.ch/AccwConf/f05/PAPERS/THPP038PDF.
- ⁵²Y. Ding *et al.*, "Measurements and simulations of ultralow emittance and ultrashort electron beams in the linac coherent light source," *Phys. Rev. Lett.* **102**, 254801 (2009).
- ⁵³B. Cros *et al.*, "Laser plasma acceleration of electrons with multi-PW laser beams in the frame of CILEX," *Nucl. Instrum. Methods Phys. Res., Sect. A* **740**, 27–33 (2014).
- ⁵⁴See <https://eli-laser.eu/> for Extreme Light Infrastructure (ELI).
- ⁵⁵M. Gauthier *et al.*, "High repetition rate, multi-MeV proton source from cryogenic hydrogen jets," *Appl. Phys. Lett.* **111**, 114102 (2017).
- ⁵⁶A. Poyé *et al.*, "Dynamic model of target charging by short laser pulse interactions," *Phys. Rev. E* **92**, 043107 (2015).
- ⁵⁷Y. Ping *et al.*, "Absorption of short laser pulses on solid targets in the ultra-relativistic regime," *Phys. Rev. Lett.* **100**, 085004 (2008).
- ⁵⁸See <https://gitlab.psi.ch/OPAL> for OPAL code.
- ⁵⁹A. Adelman *et al.*, "Fixes field accelerators and space charge modeling," in *Proceedings of the 61st ICF Advanced Beam Dynamics Workshop High-Intensity High-Brightness Hadron Beams*, Daejeon, South Korea, 2018, <http://www.jacow.org>, pp. 158–162.
- ⁶⁰M. E. Conde *et al.*, "Generation and acceleration of high-charge short-electron bunches," *Phys. Rev. Spec. Top.-Accel. Beams* **1**, 041302 (1998).
- ⁶¹P. Antici *et al.*, "Laser-driven electron beamlines generated by coupling laser-plasma sources with conventional transport systems," *J. Appl. Phys.* **112**, 044902 (2012).
- ⁶²A. Ben-Ismaïl *et al.*, "Compact and high-quality gamma-ray source applied to 10 μ m-range resolution radiography," *Appl. Phys. Lett.* **98**, 264101 (2011).
- ⁶³P. A. Norreys *et al.*, "Observation of a highly directional γ -ray beam from ultrashort, ultraintense laser pulse interactions with solids," *Phys. Plasmas* **6**, 2150–2156 (1999).
- ⁶⁴R. D. Edwards *et al.*, "Characterization of a gamma-ray source based on a laser-plasma accelerator with applications to radiography," *Appl. Phys. Lett.* **80**, 2129–2131 (2002).
- ⁶⁵Z.-H. He *et al.*, "Capturing structural dynamics in crystalline silicon using chirped electrons from a laser wakefield accelerator," *Sci. Rep.* **6**, 36224 (2016).
- ⁶⁶S. Palaniyappan *et al.*, "Dynamics of relativistic transparency and optical shuttering in expanding overdense plasmas," *Nat. Phys.* **8**, 763–769 (2012).
- ⁶⁷H. S. Ghotra *et al.*, "Transverse electromagnetic Hermite–Gaussian mode-driven direct laser acceleration of electron under the influence of axial magnetic field," *Laser Part. Beams* **36**, 154–161 (2018).